Improving the Attenuation of Moving Interfering Objects in Videos Using Shifted-Velocity Filtering

Chamira U. S. Edussooriya*, Dileepa Marasinghe*,†, Chamith Wijenayake‡, Len T. Bruton§ and Panajotis Agathoklis¶

*Department of Electronic and Telecommunication Engineering, University of Moratuwa, Moratuwa, Sri Lanka

†Centre for Wireless Communications, Univeristy of Oulu, Oulu, Finland

‡School of Information Technology and Electrical Engineering, University of Queensland, Brisbane, QLD, Australia

§Department of Electrical and Computer Engineering, University of Calgary, Calgary, AB, Canada

¶Department of Electrical and Computer Engineering, University of Victoria, Victoria, BC, Canada

Emails: chamira@uom.lk, dileepa.marasinghe@oulu.fi, c.wijenayake@uq.edu.au, bruton@ucalgary.ca, panagath@ece.uvic.ca

***Abstract*—Three-dimensional space-time velocity filters may be used to enhance dynamic passband objects of interest in videos while attenuating moving interfering objects based on their velocities. In this paper, we show that the attenuation of interfering stopband objects may be significantly improved using recently proposed shifted-velocity filters. It is shown that an improvement of approximately 20 dB in signal-to-interference ratio may be achieved for stopband to passband velocity differences of only 1 pixels/frame. More importantly, this improvement is achieved without increasing the computational complexity.**

***Index Terms*—3-D velocity filters, shifted-velocity filters, linear-trajectory filters, spectral transform, moving interfering objects.**

I. Introduction

Three-dimensional (3-D) velocity filters (VFs) (also known as linear-trajectory filters) are a class of 3-D spatio-temporal filters that can be employed to selectively enhance or attenuate objects moving with approximately constant velocities in videos. Such VFs find numerous applications in advanced driver assistance systems, traffic analysis, motion detection and analysis, radar tracking and the attenuation of sunlight flicker patterns [1]–[10]. Previously reported designs of VFs include both finite-extent impulse response (FIR) and infinite-extent impulse response (IIR) digital filters having planar-shaped [5], [11], [12] or wedge-shaped (i.e., exterior of a wide-angle cone) [3], [7], [8], [13], [14] passbands in the associated spatio-temporal 3-D frequency domain. We refer to these filters as *conventional VFs*.

Motivated by the architecture of the well-known *delay-and-sum beamformers* [15]–[17, ch. 6], a novel architecture for VFs has been proposed in [18] in order to reduce the computational complexity of VFs. In this architecture, the input video signal is first shifted along the two spatial dimensions using a two-dimensional (2-D) spatial variable-shift (SVS) filter prior to subsequent filtering with a 3-D FIR VF having a wedge-shaped passband. We refer to the VFs based on this architecture as *shifted VFs*. The shifted VF proposed in [18] provides approximately 60% reduction of the computational complexity compared to the state-of-the-art conventional VF having the lowest computational complexity [13]. In [10], the computational complexity of shifted VFs has been further reduced by approximately 50% (compared to the shifted VF proposed in [18]) using a 3-D IIR VF.

In this paper, we show that the attenuation of moving interfering objects (MIOs) in videos may be significantly improved using the shifted VFs. The performance of conventional VFs in attenuating MIOs significantly deteriorate when the velocity of an MIO is close to the velocity of the object of interest (OOI) to be enhanced. This happens as a result of the narrow angular separation between the spectral regions of support (ROSs) of the OOI and the MIO, which occurs when the velocities are close. Note that, in [10] and [18], only the low-complexity filter architectures for shifted VFs have been analyzed whereas, in this paper, we analyze the significantly improved attenuation of MIOs by shifted VFs using the spectral properties of moving objects in videos and verify using numerical simulations. A representative case, where the velocities of the OOI and the MIOs differ only by 1 pixels/frame indicates that the shifted VFs provide approximately 20 dB improvement in signal-to-interference ratio (SIR) compared to conventional VFs without increasing the computational complexity.

The rest of the paper is organized as follows. Spectral properties of an object moving with constant velocity is described in Section II. The attenuation performance of conventional VFs and shifted VFs are analyzed in Section III. In Section IV, the improved performance of shifted VFs are verified using extensive numerical simulations. Finally, conclusions and future work are presented in Section V.

II. Three-Dimensional Spectral Properties of an Object Moving with a Constant Velocity

The spectrum of an object moving with a constant 2-D velocity in a video (referred to as a linear-trajectory signal [11]) is briefly reviewed in this section. To this end, we consider an object moving with the constant velocity $[v_x, v_y]^{\mathrm{T}}$ $(\in \mathbb{R}^2)$ and having a time-invariant 2-D spatial intensity as shown in Fig. 1(a). In this case, the 3-D discrete-domain intensity of the moving object, $i(n_x, n_y, n_t)$, $(n_x, n_y, n_t) \in \mathbb{Z}^3$, can be expressed as [11], [19, ch. 2.3]

$$i(n_x, n_y, n_t) = i_r^{n_{t0}}(n_x - \Delta x(n_t), n_y - \Delta y(n_t)), \quad (1)$$

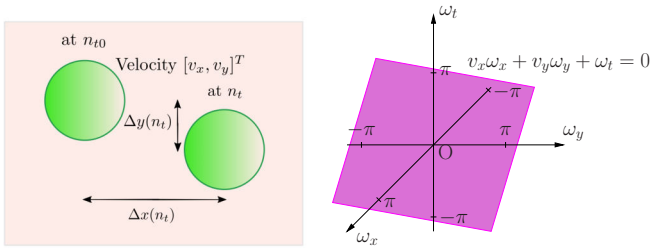

(a) (b)

Fig. 1: (a) An object moving with a constant 2-D velocity $[v_x, v_y]^{\mathrm{T}}$ and having a time-invariant 2-D spatial intensity; (b) the planar ROS of its 3-D spectrum inside the principal Nyquist cube $\mathcal{N} \in \mathbb{R}^3$.

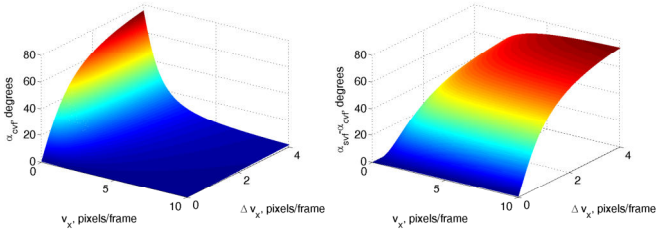

(a) (b)

Fig. 2: (a) The angle α_{cvf} between the spectral ROSs of the OOI and the MOI; (b) the difference between the angles α_{svf} and α_{cvf}.

where $i_r^{n_{t0}}(n_x, n_y)$ is the 2-D spatial intensity of the object in the *reference frame* captured at $n_t = n_{t0}$. Here, $\Delta x(n_t)$ and $\Delta y(n_t)$ are the distances corresponding to the motion of the object along the n_x and n_y discrete spatial dimensions, respectively, during $(n_t - n_{t0})$ samples, and are given by [19, ch. 2.3]

$$\Delta x(n_t) = v_x(n_t - n_{t0}) \tag{2a}$$
$$\Delta y(n_t) = v_y(n_t - n_{t0}), \tag{2b}$$

respectively. In this case, the intensity of the moving object at any time instant is a *shifted replica* of the time-invariant 2-D spatial intensity captured at the reference frame as shown in Fig. 1(a). Note that the assumption of a time-invariant 2-D spatial intensity (also know as the *constant intensity assumption* [19, ch. 2.3]) is predominantly valid for moving objects in real scenes under diffuse illumination.

The 3-D spectrum of the intensity $i(n_x, n_y, n_t)$ can be obtained as [11] [19, ch. 2.3]

$$I(\mathrm{e}^{j\omega_x}, \mathrm{e}^{j\omega_y}, \mathrm{e}^{j\omega_t}) = I_r^{n_{t0}}(\mathrm{e}^{j\omega_x}, \mathrm{e}^{j\omega_y})\, \delta(v_x\omega_x + v_y\omega_y + \omega_t), \tag{3}$$

inside the 3-D principal Nyquist cube $\mathcal{N}$, where $I_r^{n_{t0}}(\mathrm{e}^{j\omega_x}, \mathrm{e}^{j\omega_y})$ is the 2-D discrete-domain Fourier transform of $i_r^{n_{t0}}(n_x, n_y)$ and $\delta(\cdot)$ is the one-dimensional (1-D) continuous-domain impulse function. Note that $\mathcal{N} \triangleq \{(\omega_x, \omega_y, \omega_t) \in \mathbb{R}^3 \mid -\pi \leq \omega_x, \omega_y, \omega_t < \pi\}$. The ROS $\mathcal{R}$ of this 3-D spectrum, inside $\mathcal{N}$, can be obtained as

$$\mathcal{R} = \{(\omega_x, \omega_y, \omega_t) \in \mathcal{N} \mid I_r^{n_{t0}}(\mathrm{e}^{j\omega_x}, \mathrm{e}^{j\omega_y}) \neq 0 \text{ and } v_x\omega_x + v_y\omega_y + \omega_t = 0\}. \tag{4}$$

According to (4), inside $\mathcal{N}$, $\mathcal{R}$ lies on a *plane* having a normal vector $[v_x, v_y, 1]^{\mathrm{T}}$ and going through the origin [11] as shown in Fig. 1(b).

III. Attenuation of Moving Interfering Objects Using 3-D Velocity Filtering

A. Conventional Velocity Filtering

It is evident from (4) that, ideally, the spectral ROSs of objects moving with different constant velocities do not overlap except at the origin inside $\mathcal{N}$. Consequently, an OOI moving with a constant velocity can be enhanced while attenuating MIOs having velocities which are different from that of the OOI using a 3-D VF. Note that the passband of such a 3-D VF effectively encompasses the spectral ROS of the OOI while the stopband encompasses the spectral ROSs of the MIOs, thereby achieving velocity-selective filtering. In conventional VF design methods, the passband has been selected to be planar or wedge shaped and has been approximated by a 3-D FIR or IIR transfer function.

In order to analyze the performance of conventional VFs in attenuating MIOs, let us consider an OOI moving with a velocity $[v_x, v_y]^{\mathrm{T}}$ and an MIO having a velocity $[v_x + \Delta v_x, v_y + \Delta v_y]^{\mathrm{T}}$, where $\Delta v_x, \Delta v_y \in \mathbb{R}$. The angle α_{cvf} between the planar spectral ROSs of the OOI and that of the MIO can be obtained as

$$\alpha_{cvf} = \cos^{-1}\left[\frac{v_x(v_x + \Delta v_x) + v_y(v_y + \Delta v_y) + 1}{\|\mathbf{v}_{ooi}\|\,\|\mathbf{v}_{mio}\|}\right] \tag{5}$$

using the dot product between the two vectors $\mathbf{v}_{ooi} = [v_x, v_y, 1]^{\mathrm{T}}$ and $\mathbf{v}_{mio} = [v_x + \Delta v_x, v_y + \Delta v_y, 1]^{\mathrm{T}}$, where $\|\cdot\|$ denotes the 2-norm of a vector. Note that α_{cvf} is a function of four variables: v_x,v_y,Δv_x, and Δv_y. In order to observe the variation of α_{cvf} with respect to the velocities of the OOI and the MIO, α_{cvf} is calculated for a representative case, where $v_y, \Delta v_y = 0$ pixels/frame and is shown in Fig. 2(a). Note that, in this case, α_{cvf} depends only on v_x and Δv_x. It can be observed that α_{cvf} *rapidly decreases* with v_x. In particular, when the velocity of the MIO is close to that of the OOI, i.e., $\Delta v_x \leq 1$ pixels/frame, $\alpha_{cvf} < 10^\circ$ if $v_x \geq 2$ pixels/frame and $\alpha_{cvf} < 5^\circ$ if $v_x \geq 3$ pixels/frame. Similar behavior of α_{cvf} can be observed in the more general cases, where $v_x, v_y, \Delta v_x, \Delta v_y \neq 0$ pixels/frame. When α_{cvf} is close to 0°, the VF should have a very sharp transition band in order to effectively attenuate the MIO. As a result, the order of the VF needs to be *significantly increased leading to a higher computational complexity and higher group delay*, which are undesirable, especially in real-time applications.

B. Shifted-Velocity Filtering

We now show that MIOs having velocities close to that of the OOI can be significantly attenuated using shifted VFs compared to conventional VFs without compromising the computational complexity. To this end, we consider the

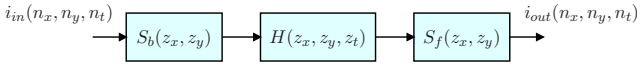

Fig. 3: Structure of a shifted VF.

structure of a shifted VF shown in Fig. 3. Here, $H(z_x, z_y, z_t)$, $(z_x, z_y, z_t) \in \mathbb{C}^3$, is a 3-D filter having a planar-shaped or wedge-shaped [10], [18] passband, which *encompasses the* $\omega_t = 0$ *plane* inside $\mathcal{N}$, and $S_b(z_x, z_y)$ and $S_f(z_x, z_y)$, $(z_x, z_y) \in \mathbb{C}^2$, are 2-D SVS filters. In order to describe the operation of a shifted VF, let us consider a video signal $i_{in}(n_x, n_y, n_t)$ consisting of an OOI and an MIO having intensities $i_{ooi}(n_x, n_y, n_t)$ and $i_{mio}(n_x, n_y, n_t)$, respectively, and moving with velocities $[v_x, v_y]^{\mathrm{T}}$ and $[v_x + \Delta v_x, v_y + \Delta v_y]^{\mathrm{T}}$, respectively. Note that $i_{in}(n_x, n_y, n_t) = i_{ooi}(n_x, n_y, n_t) + i_{mio}(n_x, n_y, n_t)$. The 2-D SVS filter $S_b(z_x, z_y)$ spatially shifts $i_{in}(n_x, n_y, n_t)$ by $-\Delta x_{ooi}(n_t)$ and $-\Delta y_{ooi}(n_t)$ (see (2a) and (2b)) along the n_x and n_y, dimensions, respectively. In fact, $S_b(z_x, z_y)$ performs the affine transform given by

$$\begin{bmatrix} \widehat{n}_x \\ \widehat{n}_y \\ \widehat{n}_t \end{bmatrix} = \begin{bmatrix} 1 & 0 & -v_x \\ 0 & 1 & -v_y \\ 0 & 0 & 1 \end{bmatrix} \begin{bmatrix} n_x \\ n_y \\ n_t \end{bmatrix} + \begin{bmatrix} v_x n_{t0} \\ v_y n_{t0} \\ 0 \end{bmatrix}, \tag{6}$$

where $(\widehat{n}_x, \widehat{n}_y, \widehat{n}_t) \in \mathbb{Z}^3$. Note that, after this affine transform, the apparent velocity of the OOI is $[0, 0]^{\mathrm{T}}$ and that of the MIO is $[\Delta v_x, \Delta v_y]^{\mathrm{T}}$. Consequently, the OOI appears to be *stationary* with respect to the temporal dimension whereas the MIO appears to be moving with $[\Delta v_x, \Delta v_y]^{\mathrm{T}}$. The 2-D SVS filter $S_f(z_x, z_y)$ is employed to reintroduce the motion of the OOI after filtering with $H(z_x, z_y, z_t)$. That is, $S_f(z_x, z_y)$ spatially shifts the output of $H(z_x, z_y, z_t)$ by $\Delta x_{ooi}(n_t)$ and $\Delta y_{ooi}(n_t)$ along the n_x and n_y, dimensions, respectively.

The corresponding transform in the frequency domain is linear inside $\mathcal{N}$ and is given by

$$\begin{bmatrix} \widehat{\omega}_x \\ \widehat{\omega}_y \\ \widehat{\omega}_t \end{bmatrix} = \begin{bmatrix} 0 & 0 & 1 \\ 0 & 1 & 0 \\ v_x & v_y & 1 \end{bmatrix} \begin{bmatrix} \omega_x \\ \omega_y \\ \omega_t \end{bmatrix}, \tag{7}$$

where $(\widehat{\omega}_x, \widehat{\omega}_y, \widehat{\omega}_t) \in \mathbb{R}^3$. Note that the spectral ROS of $i_{ooi}(\widehat{n}_x, \widehat{n}_y, \widehat{n}_t)$ lies on the $\widehat{\omega}_t = 0$ plane (having the normal vector $\widehat{\mathbf{v}}_{ooi} = [0, 0, 1]^{\mathrm{T}}$) whereas that of the $i_{mio}(\widehat{n}_x, \widehat{n}_y, \widehat{n}_t)$ lies on the plane having the normal vector $\widehat{\mathbf{v}}_{mio} = [\Delta v_x, \Delta v_y, 1]^{\mathrm{T}}$ inside $\mathcal{N}$. More importantly, this linear transform is *a shear (or skew) rather than a rotation*. Therefore, the angle α_{svf} between the spectral ROSs of the OOI and the MIO is different from α_{cvf} in (5) and can be obtained as

$$\alpha_{svf} = \cos^{-1}\left[\frac{1}{\|\widehat{\mathbf{v}}_{mio}\|}\right]. \tag{8}$$

Note that α_{svf} depends only on Δv_x and Δv_y, and is significantly greater than α_{cvf} when the velocity of the MIO is close to that of the OOI. For example, for the case $\Delta v_x = 1$ and $\Delta v_y = 0$ pixels/frame, $\alpha_{svf} = 45°$. Fig. 2(b) shows $\alpha_{svf} - \alpha_{cvf}$ for the representative case considered in Sec. III-A. It can be observed that $(\alpha_{svf} - \alpha_{cvf}) > 25°$ when $\Delta v_x \geq 1$ and $v_x \geq 1$ pixels/frame. *This indicates a significant angular separation between the spectral ROSs of the OOI and the MIO in the shifted-velocity filtering compared to the conventional velocity filtering*. Consequently, the transition band of $H(z_x, z_y, z_t)$ can be wider compared to that of a conventional VF. In this case, the $H(z_x, z_y, z_t)$ can be approximated with relatively lower order leading to a lower computational complexity and a group delay. On the other hand, if both $H(z_x, z_y, z_t)$ and the conventional VF have the same order, hence similar transition bands, the MIO is significantly attenuated by the former compared to the latter because, in this case, the spectral ROS of the MIO lies predominantly in the stopband of $H(z_x, z_y, z_t)$.

It is worthwhile to note that the 2-D SVS filters $S_b(z_x, z_y)$ and $S_f(z_x, z_y)$ can be implemented with 2-D shifts with *no arithmetic operations* [10], [18] if $\Delta x_{ooi}(n_t)$ and $\Delta y_{ooi}(n_t)$ are integer-valued, i.e., the motion is quantized to pixel level, discarding fractions. Because wedge-shaped passbands are *robust to motion estimations errors*, the effect of this quantization is negligible on the performance of the shifted VFs as verified in [10]. In practice, $\Delta x_{ooi}(n_t)$ and $\Delta y_{ooi}(n_t)$ can be estimated by means of readily available motion estimation techniques [19, ch. 6].

IV. Verification Using Numerical Simulations

In this section, we numerically verify that shifted VFs significantly outperform conventional VFs in attenuating MIOs having velocities close to that of the OOI. To this end, a *standard test video signal* containing an OOI and an MIO having checkerboard intensity patterns [10], [13], [18] is numerically generated. Furthermore, the energy of the OOI and the MIO are selected to be the same (thus the input SIR $= 0$ dB) and the size of the test video is $512 \times 512 \times 41$.

Both the conventional velocity filter and the filter $H(z_x, z_y, z_t)$ of the shifted VF are designed as 3-D FIR frequency planar filters. We employ planar-shaped passbands because both a conventional VF and a shifted VF having similar passband shapes can be designed ensuring a fair comparison. Note that the filter-bank based design methods proposed in [10], [18] for shifted VFs cannot be used to design conventional VFs. The filter $H(z_x, z_y, z_t)$ is designed by cascading three 1-D lowpass filters (i.e., $H(z_x, z_y, z_t) = H_x(z_x)H_y(z_y)H_t(z_t)$) and the conventional VF $C(z_x, z_y, z_t)$ is designed by rotating the passband of $H(z_x, z_y, z_t)$ to the required orientation [20]. Due to the limited space, we do not present the rotation-based 3-D filter design method, and the reader is referred to [20] for more details. The 1-D lowpass filters $H_x(z_x)$, $H_y(z_y)$ and $H_t(z_t)$ are designed using the windowing method with Hamming windows [21, ch. 9], and the bandwidths are selected to be 0.9π, 0.9π and 0.05π rad/sample, respectively. Note that, instead of the Hamming window, other windows such as von Hann, Kaiser and Dolph-Chebyshev [21, ch. 9] can be employed. The -3 dB isosurfaces of the magnitude responses of $H(z_x, z_y, z_t)$ and $C(z_x, z_y, z_t)$ designed to enhance an OOI moving with the velocity $[3, 7]^{\mathrm{T}}$ pixels/frame are shown in Fig. 4.

TABLE I: The output SIRs (in dB) achieved with the conventional and the shifted VFs.

Velocity of the OOI	$[3,7]^{\mathrm{T}}$	$[1,-2]^{\mathrm{T}}$	$[6,-3]^{\mathrm{T}}$	$[-7,-6]^{\mathrm{T}}$	$[2,3]^{\mathrm{T}}$	$[0,-1]^{\mathrm{T}}$	$[7,4]^{\mathrm{T}}$	$[-4,6]^{\mathrm{T}}$	$[-1,-3]^{\mathrm{T}}$	$[5,-8]^{\mathrm{T}}$
Velocity of the MIO	$[4,6]^{\mathrm{T}}$	$[0,-2]^{\mathrm{T}}$	$[7,-1]^{\mathrm{T}}$	$[-5,-8]^{\mathrm{T}}$	$[4,4]^{\mathrm{T}}$	$[1,-2]^{\mathrm{T}}$	$[7,6]^{\mathrm{T}}$	$[-3,8]^{\mathrm{T}}$	$[-1,-4]^{\mathrm{T}}$	$[6,-7]^{\mathrm{T}}$
Conventional VF	1.82	5.07	4.99	0.37	8.65	10.18	2.45	4.28	1.30	1.29
Shifted VF	11.20	21.27	27.29	12.40	27.29	11.20	39.05	27.29	21.27	11.20

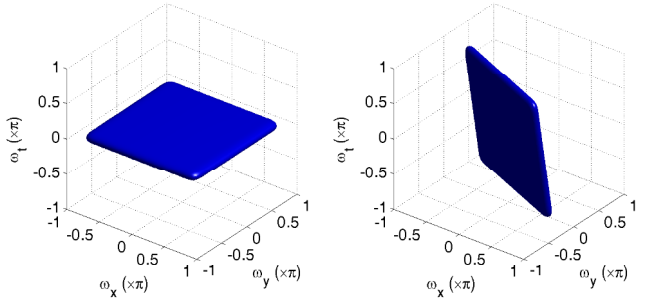

(a) (b)

Fig. 4: The -3 dB isosurfaces of the magnitude responses of (a) the shifted VF $H(z_x, z_y, z_t)$ and (b) the conventional VF $C(z_x, z_y, z_t)$. The order of both filters is $20 \times 20 \times 20$.

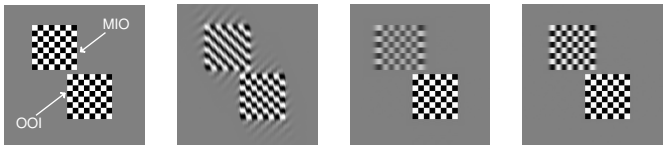

(a) (b) (c) (d)

Fig. 5: A selected region of the 21st frame of (a) the input video; the outputs of the (b) conventional VF of order $20 \times 20 \times 20$ (c) shifted VF of order $20 \times 20 \times 20$ and (d) shifted VF of order $10 \times 10 \times 10$.

As representative cases, eight test video signals are used in the first part of the simulations. The velocities of the OOI and the MIO are selected as $[v_x, 5]^{\mathrm{T}}$ and $[v_x+1, 5]^{\mathrm{T}}$ pixels/frame, where $v_x = 1, 2, \ldots, 8$. The test video signals are processed with a conventional VF of order $20 \times 20 \times 20$ and two shifted VFs of orders $20 \times 20 \times 20$ and $10 \times 10 \times 10$. A selected region of the 21st frame of the input video corresponding to $v_x = 2$ pixels/frame and the processed videos are shown in Fig. 5. It can be observed that the conventional VF fails to attenuate the MIO whereas the shifted VF of order $20 \times 20 \times 20$ considerably attenuates the MIO and that of order $10 \times 10 \times 10$ substantially attenuates the MIO. Furthermore, the OOI is substantially distorted in the output of the conventional VF whereas negligible distortion is introduced by both shifted VFs. In order to quantitatively evaluate the attenuation performance, SIRs at the outputs of the VFs are calculated and presented in Fig. 6. The average output SIRs of the conventional VF, the shifted VF of order $20 \times 20 \times 20$ and the shifted VF of order $10 \times 10 \times 10$ are 1.54, 21.27 and 7.58 dB, respectively. Note that the output SIR of the two shifted VFs are independent of v_x because $[\Delta v_x, \Delta v_y]^{\mathrm{T}} = [1, 0]^{\mathrm{T}}$ for all the cases. Accordingly, approximately 20 dB improvement in SIR is provided by the shifted VF compared to the conventional VF having the same order. Importantly, the lower order shifted VF

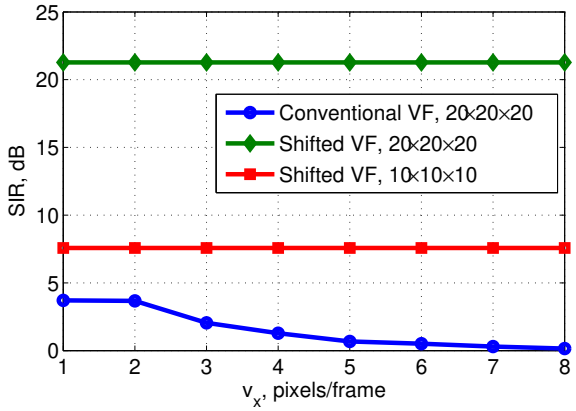

Fig. 6: The output SIRs achieved with the conventional VF and the two shifted VFs.

outperforms the conventional VF by approximately 6 dB.

Ten video signals that represent more general cases are used in the second part of the simulations. The ten video signals are processed with a conventional VF and a shifted VF. The order of both VFs is $20 \times 20 \times 20$. The velocities of the OOI and the MIO, and the achieved output SIRs are presented in Table I. It can be observed that the shifted VF provides more than 9 dB improvement in SIR compared to the conventional VF for the cases where $|v_x| > 1$ or $|v_y| > 1$ pixels/frame. In the case 6, the performance of both filters are similar because the angular separation between the spectral ROSs of the OOI and the MIO are similar for both velocity filtering methods when $|v_x|, |v_y| \leq 1$ pixels/frame (see Figs. 2(a) and 2(b)).

V. Conclusion and Future Work

Novel use of 3-D shifted VFs is proposed for the selective enhancement of moving objects in video signals in the presence of the MIOs having relatively close velocities to that of the OOI. The proposed approach addresses a major limitation in conventional VFs which shows degraded performance when the angular separation between the planar spectral ROSs of an OOI and an MIO is very small. Numerical simulations verify that the proposed shifted VFs provide significant improvement in SIR compared to conventional VFs when $|v_x| > 1$ or $|v_y| > 1$ pixels/frame, importantly without compromising the computational complexity. Future work includes extension of the shifted VF architecture to four-dimensional depth filters [22]–[24] and five-dimensional depth-velocity filters [25]–[27] for light field and light field video processing, respectively, in such applications as virtual reality and computational photography.

Acknowledgment

Authors thank the University of Moratuwa and the University of Queensland for financial support.

REFERENCES

[1] T. J. Fowlow and L. T. Bruton, "The design and application of a high quality three dimensional linear trajectory filter," in *Proc. IEEE Int. Symp. Circuits Syst.*, 1988, pp. 1033–1036.

[2] L. T. Bruton, N. R. Bartley, and Z. Q. Liu, "On the classification of moving objects in image sequences using 3D adaptive recursive tracking filters and neural networks," in *Proc. 29th Asilomar Conf. Signals, Syst., Comput.*, vol. 2, 1995, pp. 1006–1010.

[3] K. Kondo and N. Hamada, "Design of optimal filter for detecting linear trajectory signals utilizing object shape and velocity vector," *Electron. and Commun. in Japan, Part I*, vol. 83, no. 2, pp. 42–51, Feb. 2000.

[4] J.-Y. Chang, C.-C. Cheng, S.-Y. Chien, and L.-G. Chen, "Relative depth layer extraction for monoscopic video by use of multidimensional filter," in *Proc. IEEE Int. Conf. Multimedia and Expo*, 2006, pp. 221–224.

[5] S.-C. Pei, W.-Y. Kuo, and W.-T. Huang, "Tracking moving objects in image sequences using 1-D trajectory filter," *IEEE Signal Process. Lett.*, vol. 13, no. 1, pp. 13–16, Jan. 2006.

[6] S. Schauland, J. Velten, and A. Kummert, "Multidimensional linear shift invariant velocity filters for vision-based automotive applications," in *Proc. Int. Workshop Multidim. (nD) Syst.*, 2007, pp. 83–87.

[7] ——, "Detection of moving objects in image sequences using 3D velocity filters," *Int. J. Appl. Math. Comput. Sci.*, vol. 18, no. 1, pp. 21–31, Mar. 2008.

[8] T. Schwerdtfeger, J. Velten, and A. Kummert, "A multidimensional wave digital filter bank for video-based motion analysis," *Multidim. Syst. Signal Processing*, vol. 25, no. 2, pp. 295–311, Apr. 2014.

[9] H. L. Kennedy, "Multidimensional digital filters for point-target detection in cluttered infrared scenes," *J. Electron. Imag.*, vol. 23, no. 6, pp. 063 019–1–063 019–11, Nov./Dec. 2014.

[10] C. U. S. Edussooriya, L. T. Bruton, and P. Agathoklis, "Velocity filtering for attenuating moving artifacts in videos using an ultra-low complexity 3-D linear-phase IIR filter," *Multidim. Syst. Signal Process.*, vol. 28, no. 2, pp. 597–616, Apr. 2017.

[11] L. T. Bruton and N. R. Bartley, "Three-dimensional image processing using the concept of network resonance," *IEEE Trans. Circuits Syst.*, vol. CAS-32, no. 7, pp. 664–672, July 1985.

[12] L. T. Bruton and N. Bartley, "The enhancement and tracking of moving objects in digital images using adaptive three-dimensional recursive filters," *IEEE Trans. Circuits Syst.*, vol. CAS-33, no. 6, pp. 604–612, June 1986.

[13] B. Kuenzle and L. T. Bruton, "3-D IIR filtering using decimated DFT-polyphase filter bank structures," *IEEE Trans. Circuits Syst. I*, vol. 53, no. 2, pp. 394–408, Feb. 2006.

[14] B. Anderson and L. T. Bruton, "Non-uniform bandwidth frequency-planar (NUB-FP) filter banks," in *Proc. IEEE Int. Symp. Circuits Syst.*, vol. 1, 2002, pp. I–809–I–812.

[15] B. D. Van Veen and K. M. Buckley, "Beamforming: A versatile approach to spatial filtering," *IEEE ASSP Mag.*, vol. 5, no. 2, pp. 4–24, Apr. 1988.

[16] C. U. S. Edussooriya, L. T. Bruton, M. A. Naeini, and P. Agathoklis, "Using 1-D variable fractional-delay filters to reduce the computational complexity of 3-D broadband multibeam beamformers," *IEEE Trans. Circuits Syst. II*, vol. 61, no. 4, pp. 279–283, Apr. 2014.

[17] D. E. Dudgeon and R. M. Mersereau, *Multidimensional Digital Signal Processing*. Englewood Cliffs, NJ: Prentice-Hall, 1984.

[18] C. U. S. Edussooriya, L. T. Bruton, and P. Agathoklis, "A low-complexity 3D spatio-temporal FIR filter for enhancing linear trajectory signals," in *Proc. IEEE Int. Conf. Acoust., Speech, Signal Process.*, 2014, pp. 1165–1169.

[19] Y. Wang, J. Ostermann, and Y.-Q. Zhang, *Video Processing and Communications*. Upper Saddle River, NJ: Prentice-Hall, 2002.

[20] S.-C. Pei and S.-B. Jaw, "Two-dimensional general fan-type FIR digital filter design," *Signal Process.*, vol. 37, no. 2, pp. 265–274, May 1994.

[21] A. Antoniou, *Digital Signal Processing: Signals, Systems and Filters*. NY: McGraw-Hill, 2006.

[22] D. Dansereau and L. T. Bruton, "A 4D frequency-planar IIR filter and its application to light field processing," in *Proc. IEEE Int. Symp. Circuits Syst.*, vol. 4, 2003, pp. IV–476–IV–479.

[23] ——, "A 4-D dual-fan filter bank for depth filtering in light fields," *IEEE Trans. Signal Process.*, vol. 55, no. 2, pp. 542–549, Feb. 2007.

[24] N. Liyanage, C. Wijenayake, C. Edussooriya, A. Madanayake, P. Agathoklis, L. T. Bruton, and E. Ambikairajah, "Multi-depth filtering and occlusion suppression in 4-D light fields: Algorithms and architectures," *Signal Process.*, vol. 167, pp. 1–13, Feb. 2020.

[25] C. U. S. Edussooriya, D. G. Dansereau, L. T. Bruton, and P. Agathoklis, "Five-dimensional depth-velocity filtering for enhancing moving objects in light field videos," *IEEE Trans. Signal Process.*, vol. 63, no. 8, pp. 2151–2163, Apr. 2015.

[26] C. U. S. Edussooriya, L. T. Bruton, and P. Agathoklis, "A novel 5-D depth-velocity filter for enhancing noisy light field videos," *Multidim. Syst. Signal Process.*, vol. 28, no. 1, pp. 353–369, Jan. 2017.

[27] C. Wijenayake, N. Liyanage, C. U. S. Edussooriya, H. Seatang, P. Agathoklis, and L. Bruton, "Design and implementation of 5-D IIR depth velocity filters for light field video processing," *IEEE Trans. Circuits Syst. II*, vol. 66, no. 7, pp. 1267–1271, Jul. 2019.